NANO LETTERS

pubs.acs.org/NanoLett

Letter

# Facile Synthesis of Biocarbon-Based $MoS_2$ Composite for High-Performance Supercapacitor Application

Hansa Mahajan, Kannan Udaya Mohanan, and Seongjae Cho*

Cite This: *Nano Lett.* 2022, 22, 8161−8167

Read Online

ACCESS | Metrics & More | Article Recommendations | Supporting Information

**ABSTRACT:** Nanocomposites are gaining high demand for the development of next-generation energy storage devices because of their eco-friendly and cost-effective natures. However, their short-term energy retainability and marginal stability are regarded as hindrances to overcome. In this work, we demonstrate a high-performance supercapacitor fabricated by biocarbon-based $MoS_2$ (Bio-C/$MoS_2$) nanoparticles synthesized by a facile hydrothermal approach using date fruits. Here, we report the high specific capacitance for a carbon-based nanocomposite employing the pyrolysis technique of converting agricultural biowaste into a highly affordable energy resource. The biocompatible Bio-C/$MoS_2$ nanospheres exhibited a high capacitance of 945 F $g^{-1}$ at a current density of 0.5 A $g^{-1}$ and an excellent reproducing stability of 92% after 10000 charge/discharge cycles. In addition, the Bio-C/$MoS_2$ NS showed an exceptional power density of 3800−8000 W $kg^{-1}$ and an energy density of 74.9−157 Wh $kg^{-1}$. The results would pave a new strategy for design of eco-friendly materials toward the high-performance energy storage technology.

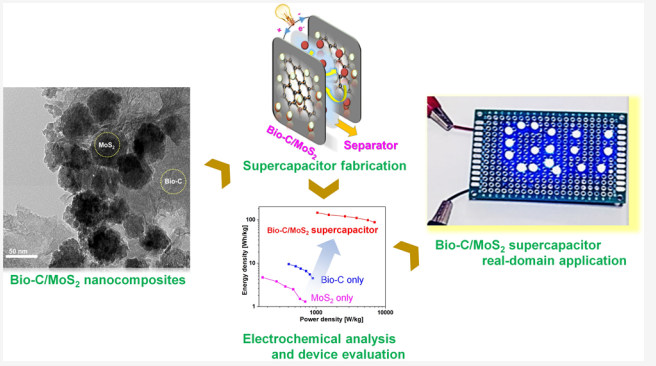


**KEYWORDS:** *biocarbon, $MoS_2$ composite, supercapacitors, nanocomposite electrodes, hydrothermal synthesis*

The rapid depletion of fossil fuels and the rampant environmental pollution arising from their excessive use have inspired researchers to work toward the development of alternative and renewable energy technologies. Meeting the sustainable energy goals of the present century requires the development of advanced energy storage technologies that comply with green standards. Recently, supercapacitors have attracted research interest because of their excellent power density, cycling life, stability, and environmental safety.[1−5] Because of their unique energy storage mechanisms, these devices are highly suitable for hybrid electric vehicles.

There are two types of supercapacitors based on energy mechanisms: electrical double-layer capacitors (EDLCs) and pseudocapacitors.[6,7] EDLC electrodes are based on carbon materials. On the other hand, pseudocapacitor electrodes are made from transition-metal oxides (TMO) and transition-metal sulfides (TMS), which store charges by their rapid and reversible Faradaic behavior aimed at high specific capacitance.[8,9] TMO, such as $RuO_2$, NiO, $MoS_2$, and $MnO_2$, have been extensively investigated for their pseudocapacitor output in aqueous $Na_2SO_4$ electrolyte.[10] Among these compounds, molybdenum disulfide ($MoS_2$) is a well-known electrode material used for energy conservation.[11,12] $MoS_2$ is not just employed for lithium-ion batteries as a layered assembly, but it also has potential in pseudocapacitors because the oxidation state of Mo can range from +2 to +6. The theoretical capacitance of $MoS_2$ is 1403 F $g^{-1}$.[13] However, obtaining this theoretical capacitance is challenging because of the crystallinity and bounded conductivity. In addition, the long-term cycle stability and strong rate ability of the electrolyte are major issues with pristine $MoS_2$ materials.

There are two methods for overcoming these drawbacks. The primary method is to apply the metal phase of $MoS_2$, which can provide good charge transport for a high specific capacitance.[14] The other method is the assembly of a composite material, which could be a breakthrough for the application of $MoS_2$ as a high-capacitance storage device. TMO composites with carbon-based materials such as reduced graphene oxide (RGO), carbon fibers, and biomass are excellent candidates as supercapacitor electrodes due to the low cost, ease of accessibility, biodegradable nature, and porosity of the carbon constituent.[15,16] Various types of spongy carbon have been synthesized using Cassia fistula extract, potato peel, fruit extract, coconut shell, human hair, and mammal feathers as carbon-based prototypes for biomass.[17,18] In addition, they demonstrate excellent supercapacitor

**Received:** July 1, 2022
**Revised:** September 30, 2022
**Published:** October 4, 2022

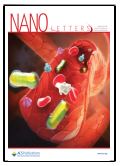





https://doi.org/10.1021/acs.nanolett.2c02595
*Nano Lett.* 2022, 22, 8161−8167

performance in acidic, basic, and neutral forms. Biomass-related carbon capacitance is strongly dependent on the phytoconstituents present in biomass. Furthermore, carbon-based materials can have a wide range of features, including large surface area, structural stability, and excellent thermal as well as optical properties. Carbon-based materials with these beneficial properties are successful in a variety of applications including energy storage and fuel cells.[19−21] Carbon-based materials are well-known for increasing the electrical conductivity, while also providing structural support to prevent metal oxide agglomeration.[22] Several composites have been reported, such as $MoS_2$/reduced graphene, aerogel, and $MoS_2$/carbon nanotube (CNT) composites.[23] The synthesis of new biocarbon-based $MoS_2$ (Bio-C/$MoS_2$) composites using single precursors is of interest for future applications.

In this study, Bio-C/$MoS_2$ nanoparticles were synthesized by a facile hydrothermal approach employing date fruit peels and seeds as raw materials. Layered date peels contain porous carbon with essential active sites, and biocarbon has major benefits over graphene sheets. Bare $MoS_2$ nanospheres (30 nm) nucleated on the carbon complex, producing a uniform size without disturbing the crumpled carbon fiber. The Bio-C/$MoS_2$ composite had a very high capacitance of 945 F $g^{-1}$ at a current density of 0.5 A $g^{-1}$, which is 3−5 times higher than that of pristine $MoS_2$ nanospheres and biocarbon electrodes. Exceptionally high energy densities ranging above 157.9 Wh $kg^{-1}$ and a high power density of 8000 W $kg^{-1}$ were achieved. Our approach provides a new path for transforming waste into precise nanoparticles without the production of secondary trash.

The morphologies and structures of the pure biocarbon, bare $MoS_2$ nanospheres, and Bio-C/$MoS_2$ composite were studied using HR-TEM, selected area electron diffraction (SAED) and STEM elemental analyses. The particle size in the $MoS_2$ nanosphere was roughly 50−100 nm, as shown in Figure 1a. HR-TEM and SAED patterns obtained for the biocarbon are shown in Figures 1b and 1c. Meanwhile, the TEM and HR-TEM images of the Bio-C/$MoS_2$ composite (Figure 1d−f) indicate that C atoms were wrapped by the $MoS_2$ nanospheres. The $MoS_2$ lattice spacing was 0.5 nm, as shown in the HR-TEM images of the Bio-C/$MoS_2$ composite, corresponding to the (110) plane of $MoS_2$. Figure 1f shows the SAED patterns of the composite, which validates the high crystallinity of the $MoS_2$ and biocarbon nanocomposites. Furthermore, the SAED pattern exhibited various sets of diffraction signals corresponding to $MoS_2$ and Bio-C hexagonal-phase planes, which can be indexed to the (002), (100), and (110) planes of $MoS_2$, and the diffraction of the (103) plane assigned to Bio-C can also be observed. In addition, STEM elemental mapping of the $MoS_2$ composite (Figure 1g−j) reveals that many $MoS_2$ nanoparticles were completely covered in activated carbon, resulting in a high density of activation sites. Elemental mapping reveals the presence of Mo, C, and S. The bright-field image of the composite also indicated that $MoS_2$ nanoparticles were decorated on the activated carbon (Figure 1k,l). Moreover, the nanocomposites produce homogeneous interconnection.[24−27] Figure 2 schematically shows the synthesis of the Bio-C/$MoS_2$ composites.

Curves i−iii in Figure 3a show the plots in comparison to the equivalent energy and power densities for Bio-C/MoS2 composites, Bio-C, and bare $MoS_2$ nanosphere capacitors, respectively, using eqs 6 and 7 in the Supporting Information. Also, further comparison is made with the recently reported

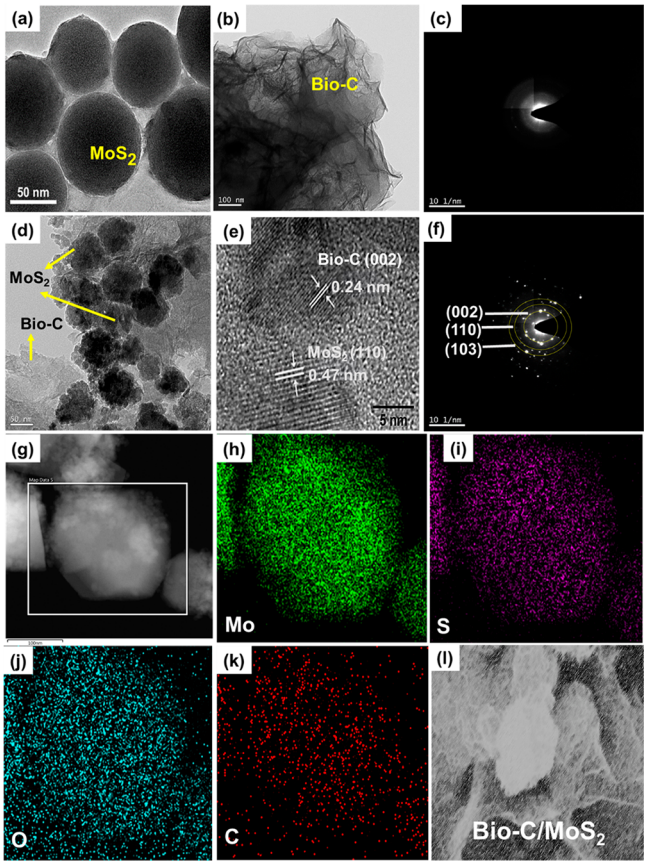


**Figure 1.** TEM, HR-TEM, and SAED images of crystalline (a) $MoS_2$ nanosphere, (b, c) Bio-C, and (d−f) Bio-C/$MoS_2$ composite. (g−l) STEM elemental mapping of Bio-C/$MoS_2$ composite.

results.[28,28−33] It was reported in an existing literature that excess oxygen content could block the pores in the active electrodes, leading to degradation in electrochemical performances.[31] The energy-dispersive spectroscopy (EDS) analysis results in Figure S4b demonstrate that the oxygen content is substantially low and does not disturb the performances. Also, the results indicate that the oxygen functional groups, carboxyl and carbonyl groups in particular, increased the wettability of the pore surfaces, diffusion velocity across the electrolyte toward the electrodes, and the specific capacitance. The oxygen functional group has a significant influence on capacitor performances and can generate pseudocapacitive behaviors via reversible redox reaction increasing the effective capacitance in overall. The mass of the as-prepared electrode material was used to calculate the energy and power densities. The Bio-C/$MoS_2$ composite had energy and power densities of 157.9 Wh $kg^{-1}$ and 8000 W $kg^{-1}$, respectively, which were much higher compared to those of bare $MoS_2$ nanosphere and Bio-C electrodes. Compared to prior publications, the Bio-C/$MoS_2$ composite electrode exhibits high energy and power densities, making it a promising candidate for high-performance electrochemical capacitors.[34]

Although the three-electrode aqueous electrolytic approach does not meet our device fabrication goals, we must investigate the feasibility of using a Bio-C/$MoS_2$ composite electrode as a solid-state device. The positive and negative electrodes of the symmetric supercapacitor were made of Bio-C/$MoS_2$ composite, and we investigated the effect of the nanocomposite on device construction without employing activated carbon, RGO,


https://doi.org/10.1021/acs.nanolett.2c02595
Nano Lett. 2022, 22, 8161−8167

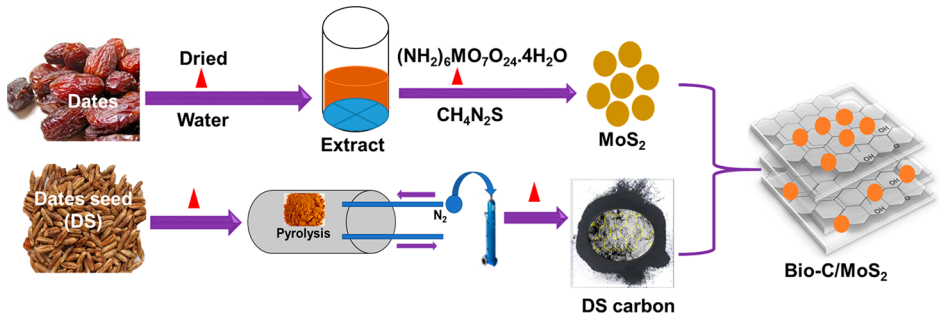


**Figure 2.** Schematic representation of the synthesis process of Bio-C/$MoS_2$ composite supercapacitor (DC carbon: date seed carbon).

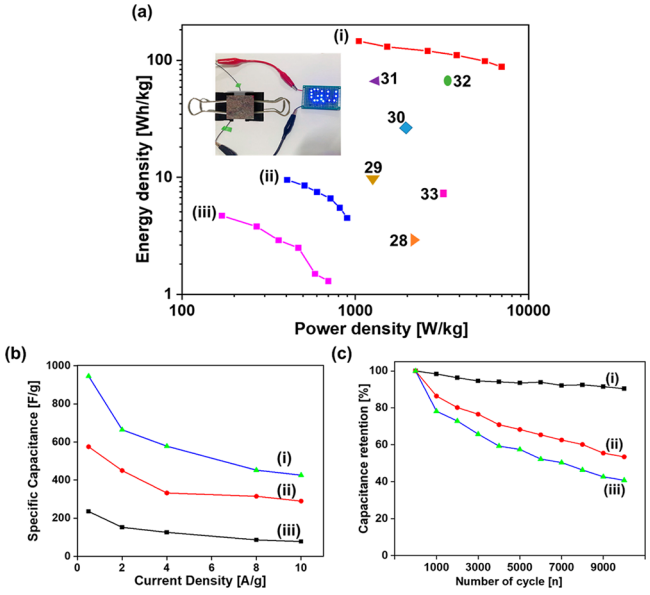


**Figure 3.** Evaluation of supercapacitor performances. (a) Ragone plot of capacitors with (i) Bio-C/$MoS_2$ composite electrodes, (ii) Bio-C electrodes, and (iii) $MoS_2$ nanosphere electrodes. The inset shows a digital photograph of brightly lit up LEDs powered by the supercapacitor with Bio-C/$MoS_2$ electrodes displaying the institute name, Gachon University (GU). (b) Specific capacitance as a function of current density. Both are normalized by mass. (c) Stability over cyclic operations of capacitors with (i) Bio-C/$MoS_2$ composite, (ii) Bio-C, and (iii) $MoS_2$ nanosphere electrodes.

or other negative electrodes. The device is depicted in a digital image in the inset of Figure 3a: 2 M $Na_2SO_4$ as the electrolyte, separator, and two Bio-C/$MoS_2$ composite electrode layers are posted together. Subsequently, the electrode was charged by connecting it to a potentiostat. The device could glow the LED, and the digital clock was powered. The inset in Figure 3a shows a digital photograph of the LED and clock powered by a Bio-C/$MoS_2$ composite two-electrode-type symmetric supercapacitor, which confirms that our device works perfectly (GU stands for the institute name).

The specific capacitance as a function of discharge current density is shown in Figure 3b. Masses of both electrodes in the supercapacitor cell were considered in calculating the current density and specific capacitance values. The mass loading of the Bio-C/$MoS_2$ composite has been identified to be around 4.13 mg for the unit electrode area, 1 $cm^2$. For comparison, the $MoS_2$ nanosphere and Bio-C were similarly tested using a capacitor-based device configuration. At the same current density, the specific capacitance of the Bio-C/$MoS_2$ composite symmetric supercapacitor was significantly larger than those of the $MoS_2$ nanosphere- and Bio-C-based electrodes. However, capacitance decreases as current density increases, which could be due to ion diffusion.[35] Furthermore, the Bio-C/$MoS_2$ composite confirms high specific capacitance values from 420.2 to 945.3 F $g^{-1}$ in Figure 3b as the current density decreases from 10 to 0.5 A $g^{-1}$ in 2 M $Na_2SO_4$ electrolytes. The mutual combination of the redox pseudocapacitance of $MoS_2$ and the EDLC of Bio-C may be responsible for the improved electrochemical capacitive performance of the Bio-C/$MoS_2$ composite supercapacitor. The nanosphere-like structure and abundant S sites of $MoS_2$ also support an increase in the specific capacitance of the Bio-C/$MoS_2$ composite electrodes. According to Brunauer-Emmett-Teller (BET) analysis results, the sphere-like shape increases the accessible surface area and porosity, resulting in a large number of ion diffusion channels and hence available sites for ion adsorption on the surface of electrode material. Furthermore, defects with unsaturated S atoms provide active sites for the electrochemical performance improvement of specific capacitance. Table S1 shows that the Bio-C/$MoS_2$ composite has one of the highest electrochemical performances among molybdenum disulfide carbon-based reported materials in terms of specific power, energy density, and capacitance. The capacitive behaviors can be attributed to the textural properties of electrode surface.[4,19,36] The results in this work can be translated in the similar way on the basis of BET analysis results in Figure S5b,d. The Bio-C/$MoS_2$ composite exhibits the type-IV isotherm curve (Figure S5b) and has a larger number of mesopores with the peak value of diameters around 4.7 nm (Figure S5d), in comparison with the case of $MoS_2$ nanospheres (Figure S5a,c). The Bio-C/$MoS_2$ composite has a smaller pore size resulting in the formation of a larger effective surface area, which is beneficial to increase in the number of active sites. It can be inferred that the specific surface area of the Bio-C/$MoS_2$ composite gets larger after adding the Bio-C nanospheres. The enlarged effective surface area of the Bio-C/$MoS_2$ composite has led to a prominent increase in specific capacitance, 945.3 F $g^{-1}$, in comparison with the case without introducing the Bio-C nanospheres, 235.2 F $g^{-1}$, as can be observed in Figure 3b. Figure 3c(i–iii) shows the cyclic stability of the bare $MoS_2$ nanosphere, Bio-C, and Bio-C/$MoS_2$ composite electrode electrochemical capacitors during charge/discharge cycles in a 2 M $Na_2SO_4$ electrolyte at 0.5 A $g^{-1}$ current density. After a 10000 cycle test, the Bio-C/$MoS_2$ composite electrode exhibited the required cycle shape and retained 92% of its primary capacitance, demonstrating the excellent eletrochemical stability of the Bio-C/$MoS_2$ composite electrode supercapacitor during the cycling test. Furthermore, from the Bio-C/$MoS_2$ composite, the sulfur bond gathered in


https://doi.org/10.1021/acs.nanolett.2c02595
Nano Lett. 2022, 22, 8161−8167

the carbon structure forms a stable covalent bond, which contributes to its outstanding stability.

Electrochemical impedance spectroscopy (EIS) is used to determine the kinetics of the electrode materials during the charging and discharging processes. To obtain the charge transfer interface, EIS analyses of bare $MoS_2$ nanosphere, Bio-C, and Bio-C/$MoS_2$ composite electrodes were conducted at a frequency of 100 down to 0.1 Hz and an amplitude of 10 mV. As illustrated in Figure 4(i–iii), the Nyquist plot depicts the real and imaginary parts of the impedance. The Nyquist plot of the as-prepared electrode shows a slanted semicircle in the high-frequency zone and a straight line almost parallel to the imaginary axis.[37] The Nyquist plot shows a narrow semicircle as depicted inset of Figure 4 for the electrode in the high-frequency region, indicating that the electrode conductivity and electrolyte ions to the electroactive components were both too low. At very high frequencies, the intercept plot on the horizontal axis denotes the equivalent series resistance, which is the combination of the electrode and electrolyte resistances at the electrode–electrolyte interface. The charge transfer resistance of the Bio-C/$MoS_2$ composite (0.5 Ω) is lower than that of $MoS_2$ (11.2 Ω) and Bio-C (2.1 Ω), as shown in Figure 4(i–iii). The accumulation of carbon improves the conductivity of the composite, which is the most important reason for the improved electrochemical performances. According to the EIS analysis results, the Bio-C/$MoS_2$ composite has a higher charge transfer capability than Bio-C and $MoS_2$ nanosphere.[38,39]

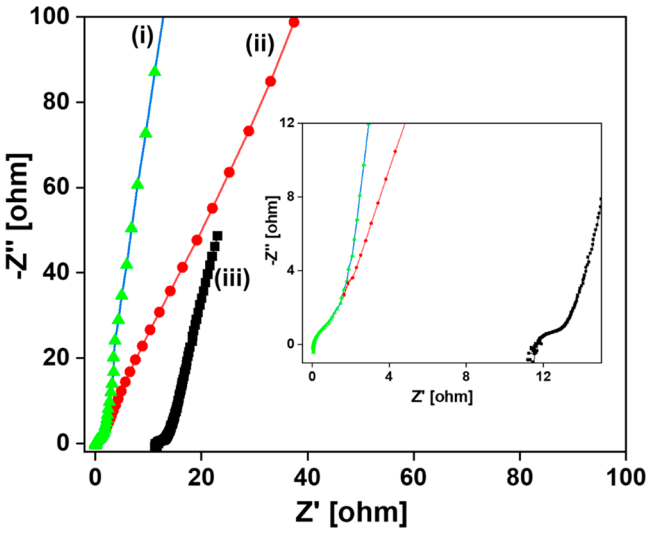


**Figure 4.** Electrochemical impedance spectra analyses from the capacitors with (i) Bio-C/$MoS_2$ composite, (ii) Bio-C, and (iii) $MoS_2$ nanosphere electrodes.

Figure 5a–c shows the cyclic voltammetry (CV) analysis of the $MoS_2$ nanosphere, Bio-C, and Bio-C/$MoS_2$ composite electrodes in a three-electrode system with an Ag/AgCl reference electrode in a 2 M $Na_2SO_4$ electrolyte at various scan speeds (20, 40, 60, 80, and 100 mV $s^{-1}$). It is reported that the increase in mass loading is directly linked to enhancement in specific capacitance in existing literature.[21,26] Here, it was pointed out that the negative effect of excessive mass loading provided only limited number of active sites and thereby reduced the overall displacement current on the electrodes. In this present work, it also has been observed that mass loading is positively related to improvements of the capacitive performances of the Bio-C/$MoS_2$ composite supercapacitor, which is evident from the CV measurement results in Figure 5a–c. It can be reassured from the previously shown EIS results in Figure 4 that the equivalent series resistance is as low as ∼0.5 Ω, which reflects that mass loading does not have a substantially negative effect on charge transport in the Bio-C/$MoS_2$ capacitor device. Figure 5a illustrates the $MoS_2$ nanosphere electrode that has a potential sweep from 0.1 to

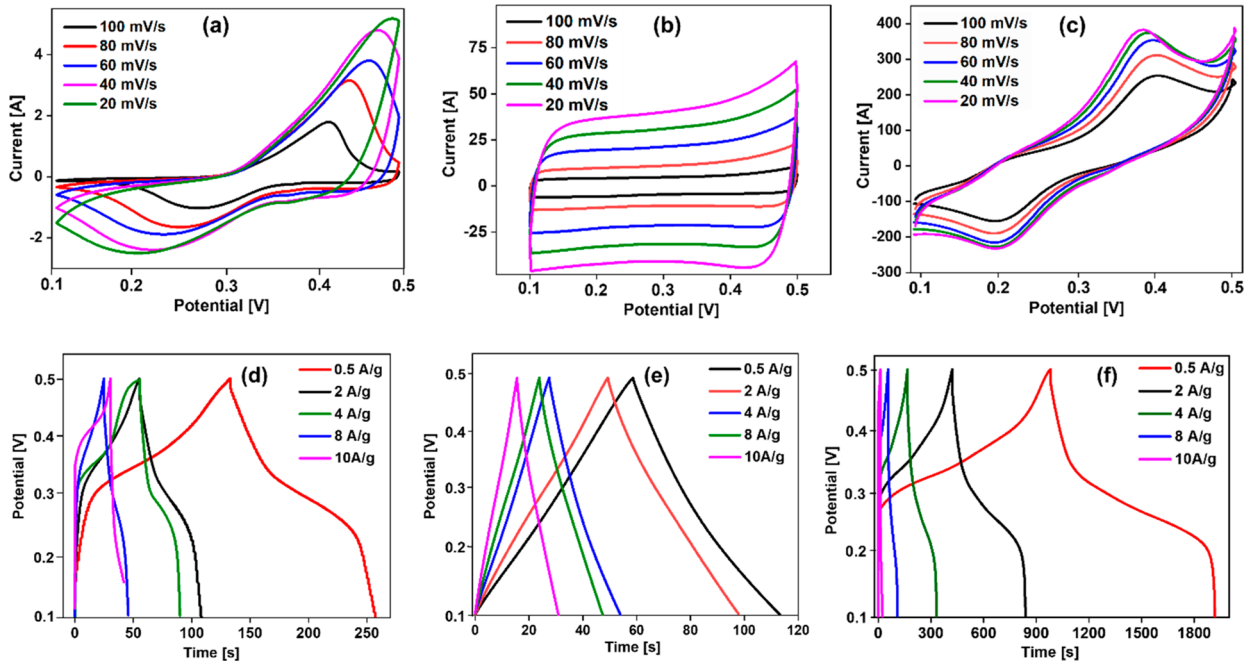


**Figure 5.** Electrochemical characterizations. (a–c) CV and (d–f) galvanostatic charge/discharge measurements from the capacitors with $MoS_2$ nanosphere (a,d), Bio-C (b,e), and Bio-C/$MoS_2$ composite electrodes (c,f) in comparison.



https://doi.org/10.1021/acs.nanolett.2c02595
Nano Lett. 2022, 22, 8161–8167

0.5 V which is very different from a rectangular shape with strong pairs of redox peaks through the anodic and cathodic peaks. A definitive redox curve can be observed in the CV curves, which signifies a typical pseudocapacitive performance caused by the existence of a reversible Faradaic reaction.[40,41] Figure 5b shows the CV of the Bio-C electrode which has confirmed a nearly rectangular structure without any noticeable redox peaks within the voltage range from 0.1 to 0.5 V, which is typical of electric double-layer charging/discharging.[42] Because of the rapid diffusion of electrolyte ions into the composite electrodes, the typical CV analysis of the Bio-C/$MoS_2$ composite (Figure 5c) revealed a highly capacitive behavior. The attachment of the $MoS_2$ nanosphere to the Bio-C sheets significantly improved the integral area of the CV peak, which improved the electrical conductivity and facilitated ion transport. Furthermore, the CV curve of the Bio-C/$MoS_2$ composite showed redox peaks aligned at 0.2 V. The redox peak of the Bio-C/$MoS_2$ composite was significantly higher than that of the bare $MoS_2$ electrodes, emphasizing the importance of biocarbon in enabling fast electron transport. Several well-defined redox peaks with Faradaic redox reactions of the $Mo^{4+}$ and $Mo^{6+}$ states (Figure S2) can be seen across the CV curve. In the $Na_2SO_4$ aqueous solution, the reaction mechanism of $MoS_2$ can be described by the following equation:

$$MoS_2 + 2Na^+ + 2e^- \leftrightarrow Na_2MoS_2$$

Charge storage occurs mainly by the insertion/removal of $Na^+$ ions into/out of the interlayer sites of carbon with $MoS_2$. The pair of peaks for the Bio-C/$MoS_2$ electrode indicates that this inter-overlapped hierarchical architecture has many easily accessible surface-redox active sites caused by the synergistic effect between the $MoS_2$ nanosphere and weakly crystalline Bio-C. These active sites are considered to be highly defective and may possess a broad distribution of energies related to surface-redox reactions. Therefore, the interaction of $Na^+$ with $MoS_2$ through the interlayer spacing of carbon may also result in high electrochemical performance. From the equation above, active $MoS_2$, $Na^+$, and electrons are incorporated into the porous carbon layer because of active site interactions and form unique pseudocapacitors. Instead of ideally rectangular shapes, the entire CV analysis has reduction and oxidation peaks, and the specific capacitance has been increased because of Faradaic pseudocapacitors, rather than pure double-layer capacitance. In addition, the relatively large surface area and high electrical conductivity may be attributed to the numerous exposed edge-rich electrochemical active sites, rapid diffusion and transport of electrolyte ions, and accelerated electrode reaction kinetics.[43] This kinetics supports the increased electrochemical performances of the Bio-C/$MoS_2$ composite in comparison to the bare $MoS_2$ nanosphere and Bio-C. On the basis of eq 5 in the Supporting Information, the specific capacitances of the Bio-C/$MoS_2$ composite at scan rates of 20, 40, 60, 80, and 100 $ms^{-1}$ were 945.3, 664.5, 577.8, 452.3, and 425.2 F $g^{-1}$, respectively. The porous structure of the resultant Bio-C/$MoS_2$ composite is most likely responsible for its considerable specific capacitance. The significant increase in capacitance is due to a positive synergistic effect in which attaching the $MoS_2$ nanospheres to the Bio-C successfully avoids the accumulation of electroactive materials, thereby reducing restacking of Bio-C sheets and thus delivering a larger electrochemically active surface area to take advantage of $MoS_2$ pseudocapacitance and biocarbon-based double-layer capacitance. The flow of ions on the outer surface of the nanoparticles may be higher, whereas the outer and inner surfaces of the material reach a low scan rate. Galvanostatic charge−discharge (GCD) analysis was performed to further evaluate the capacitive performance of the synthesized materials.[44] The galvanostatic discharge curves of the $MoS_2$ nanospheres, Bio-Cs, and Bio-C/$MoS_2$ composites at various current densities (0.5, 2, 4, 8, and 10 A $g^{-1}$) are shown in Figure 5d−f. The charge−discharge curve (Figure 5d) shows that the capacitance of $MoS_2$ nanosphere is 235.2 F $g^{-1}$ at 0.5 A $g^{-1}$. The potential of the Bio-C electrode has a linear relationship with time, indicating that it represents the EDLC characteristics. The GCD analysis of bare $MoS_2$ nanosphere reveals a triangular shape with a specific capacitance of 575.2 F $g^{-1}$ at 0.5 A $g^{-1}$ (Figure 5e). The potential vs. time graph in Figure 5f has a symmetric shape. In addition, it has a greater electroactive surface area and easy access to $OH^-$ ions for a highly viable redox reaction, and the composite Bio-C/$MoS_2$ electrode performs better (pseudocapacitors).

We adopted a one-step hydrothermal technique to produce biocarbon/molybdenum disulfide composites from natural date peels and seeds. A simple pyrolysis procedure was taken to create biocarbon fibers (Bio-C) from low-cost and eco-friendly date seeds. For the $MoS_2$ nanoparticles, the date peel extract was used as the reducing and stabilizing agent. With diameters less than 50 nm, homogeneously dispersed spheres of $MoS_2$ were successfully obtained. Structural analysis revealed that the Bio-C/$MoS_2$ composites had a nanosphere shape, which provided larger electroactive sites, and the highly porous channel structure permitted ion diffusion in the electrolyte. The capacitances of capacitors with bare $MoS_2$ nanospheres, Bio-C, and Bio-C/$MoS_2$ composite electrodes were approximately 235, 575, and 945 F $g^{-1}$, respectively, with only a 5% loss in charges after 10000 cycles at a current density of 0.5 A $g^{-1}$. The all-solid-state symmetric supercapacitor device using this nanostructured Bio-C/$MoS_2$ composite electrode has a maximum energy density of 157.9 Wh $kg^{-1}$ after 10000 cycles, with the outstanding cycling stability of 90% capacity retention. This study introduces a method for transforming waste materials for energy storage applications.

## ■ ASSOCIATED CONTENT

### Supporting Information

The Supporting Information is available free of charge at https://pubs.acs.org/doi/10.1021/acs.nanolett.2c02595.

Further background analysis results, statistical study on nanopore size, schematic of the energy storage mechanism, and comparison study in supercapacitor performances (PDF)

## ■ AUTHOR INFORMATION


### Corresponding Author

**Seongjae Cho** − *School of Electronic Engineering, Gachon University, Seongnam-si, Gyeonggi-do 13120, Republic of Korea;* orcid.org/0000-0001-8520-718X; Email: felixcho@gachon.ac.kr

### Authors

**Hansa Mahajan** − *School of Electronic Engineering, Gachon University, Seongnam-si, Gyeonggi-do 13120, Republic of Korea*




https://doi.org/10.1021/acs.nanolett.2c02595
Nano Lett. 2022, 22, 8161−8167

**Kannan Udaya Mohanan** − *School of Electronic Engineering, Gachon University, Seongnam-si, Gyeonggi-do 13120, Republic of Korea*

Complete contact information is available at: https://pubs.acs.org/10.1021/acs.nanolett.2c02595

### Author Contributions

H.M. conducted the device fabrication and electrochemical analysis and wrote the manuscript. K.U.M. checked the theoretical background and validated the experimental procedures. S.C. set up the directionality of the research, validated the mathematical, electrical, and chemical foundations from which the theoretical and empirical results are drawn, and revised the manuscript.

### Funding

This research was supported by National R&D Program through the National Research Foundation of Korea (NRF) funded by the Ministry of Science and ICT (Grant 2021M3H4A6A01048300).

### Notes

The authors declare no competing financial interest.

## REFERENCES

(1) Acerce, M.; Voiry, D.; Chhowalla, M. Metallic 1T Phase $MoS_2$ Nanosheets as Supercapacitor Electrode Materials. *Nat. Nanotechnol.* **2015**, *10*, 313−318.

(2) Zhang, N.; Li, Y.; Xu, J.; Li, J.; Wei, B.; Ding, Y.; Amorim, I.; Thomas, R.; Thalluri, S. M.; Liu, Y.; Yu, G.; Liu, L. High-performance flexible solid-state asymmetric supercapacitor based on bimetallic transition metal phosphide nanocrystals. *ACS Nano* **2019**, *13*, 10612−10621.

(3) Salanne, M.; Rotenberg, B.; Naoi, K.; Kaneko, K.; Taberna, P.-L.; Grey, C. P.; Dunn, B.; Simon, P. Efficient Storage Mechanisms for Building Better Supercapacitors. *Nat. Energy.* **2016**, *1*, 16070.

(4) Tunga, T. T.; Moussa, M.; Tripathi, K. M.; Kim, T. Y.; Nine, M. J.; Nanjundan, A. K.; Dubal, D.; Losic, D. Coupling graphene micro ribbons with carbon nanofibers: New composite hybrids for high-performing lithium and potassium-ion batteries. *Sustainable Materials and Technologies* **2022**, *32*, 2214−9937.

(5) Gogotsi, Y.; Penner, R. M. Energy storage in nanomaterials-capacitive, pseudocapacitive, or battery-like. *ACS Nano* **2018**, *12*, 2081−2083.

(6) Huo, W. C.; Dong, X.; Li, J. Y.; Liu, M.; Liu, X. Y.; Zhang, Y. X.; Dong, F. Synthesis of $Bi_2WO_6$ with Gradient Oxygen Vacancies for Highly Photocatalytic NO Oxidation and Mechanism Study. *Chem. Eng. J.* **2019**, *361*, 129−138.

(7) Geng, X.; Zhang, Y.; Han, Y.; Li, J.; Yang, L.; Benamara, M.; Chen, L.; Zhu, H. Two-Dimensional Water-Coupled Metallic $MoS_2$ with Nanochannels for Ultrafast Supercapacitors. *ACS Nano Lett.* **2017**, *17*, 1825−1832.

(8) Das, G. S.; Hwang, J. Y.; Jang, J. H.; Tripathi, K. M.; Kim, T. Biomass-Based Functionalized Graphene for Self-Rechargeable Zinc−Air Batteries. *ACS Appl. Energy Mater.* **2022**, *5*, 6663−6670.

(9) Gogotsi, Y. what Nano can do for energy storage? *ACS Nano* **2014**, *8*, 5369−5371.

(10) Mao, X.; Zou, Y.; Xu, F.; Sun, L.; Chu, H.; Zhang, H.; Zhang, J.; Xiang, C. Three-Dimensional Self-Supporting $Ti_3C_2$ with $MoS_2$ and $Cu_2O$ Nanocrystals for High-Performance Flexible Supercapacitors. *ACS Appl. Mater. Interfaces* **2021**, *13*, 22664−22675.

(11) Sahoo, D.; Shakya, J.; Choudhury, S.; Roy, S. S.; Devi, L.; Singh, B.; Ghosh, S.; Kaviraj, B. High-Performance $MnO_2$ Nanowire/$MoS_2$ Nanosheet Composite for a Symmetrical Solid-State Supercapacitor. *ACS Omega* **2022**, *7*, 16895−16905.

(12) Raza, W.; Ali, F.; Raza, N.; Luo, Y.; Kim, K. H.; Yang, J.; Kumar, S.; Mehmood, A.; Kwon, E. E. Recent Advancements in Supercapacitor Technology. *Nano Energy.* **2018**, *52*, 441−473.

(13) Yang, V.; Senthil, R. A.; Pan, J.; Khan, A.; Osman, S.; Wang, L.; Jiang, W.; Sun, Y. Highly Ordered Hierarchical Porous Carbon Derived from Biomass Waste Mangosteen Peel as Superior Cathode Material for High Performance Supercapacitor. *J. Electronal. Chem.* **2019**, *855*, 113616.

(14) Zhang, Y.; Wang, C.; Jiang, H.; Wang, Q.; Zheng, J.; Meng, C. Cobalt-Nickel Silicate Hydroxide on Amorphous Carbon Derived from Bamboo Leaves for Hybrid Supercapacitors. *Chem. Eng. J.* **2019**, *375*, 121938.

(15) Zhang, X.; Wang, Y.; Yu, X.; Tu, J.; Ruan, D.; Qiao, Z. High-Performance Discarded Separator-Based Activated Carbon for the Application of Supercapacitors. *J. Energy Storage.* **2021**, *44*, 103378.

(16) Leal da Silva, E.; Torres, M.; Portugau, P.; Cuña, A. High Surface Activated Carbon Obtained from Uruguayan Rice Husk Wastes for Supercapacitor Electrode Applications: Correlation Between Physicochemical and Electrochemical Properties. *J. Energy Storage.* **2021**, *44*, 103494.

(17) Erradi, A.; Touhtouh, S.; El Fallah, J.; El Ballouti, A.; Hajjaji, A. Performance Evaluation of Supercapacitors Based on Activated Carbons and Investigation of the Impact of Aging on the Electrodes. *J. Energy Storage.* **2021**, *40*, 102836.

(18) Cheng, F.; Yang, X.; Zhang, S.; Lu, W. Boosting the Supercapacitor Performances of Activated Carbon with Carbon Nanomaterials. *J. Power Sources.* **2020**, *450*, 227678.

(19) Jung, S. H.; Huong, P. H.; Sahani, S.; Tripathi, K. M.; Park, B. J.; Han, Y. H.; Kim, T. Y. Biomass-derived graphene-based material embedded with onion-like carbons for high power supercapacitor. *J. Electrochem. Soc.* **2022**, *169*, 010509.

(20) Wei, H.; Wang, H.; Li, A.; Li, H.; Cui, D.; Dong, M.; Lin, J.; Fan, J.; Zhang, J.; Hou, H.; Shi, Y.; Zhou, D.; Guo, Z. Advanced Porous Hierarchical Activated Carbon Derived from Agricultural Wastes Toward High-Performance Supercapacitors. *J. Alloys Compd.* **2020**, *820*, 153111.

(21) Dhiman, N.; Mohanty, P. A nitrogen and phosphorus enriched pyridine bridged inorganic-organic hybrid material for supercapacitor application. *New J. Chem.* **2019**, *43*, 16670−16675.

(22) Hao, J.; Liu, H.; Han, S.; Lian, J. $MoS_2$ Nanosheets-Polypyrrole composite deposited on reduced graphene oxide for supercapacitor. *ACS Applied Nano Mater.* **2021**, *4*, 1330−1339.

(23) Zhu, C.; Liu, T.; Qian, F.; Han, T. Y.-J.; Duoss, E. B.; Kuntz, J. D.; Spadaccini, C. M.; Worsley, M. A.; Li, Y. Supercapacitor based on three-dimensional hierarchical graphene aerogel with periodic micropores. *Nano Lett.* **2016**, *16*, 3448−3456.

(24) Sivachidambaram, M.; Vijaya, J. J.; Niketha, K.; Kennedy, L. J.; Elanthamilan, E.; Merlin, J. P. Electrochemical Studies on Tamarindus indica Fruit Shell Bio-waste Derived Nanoporous Activated Carbons for Supercapacitor Applications. *J. Nanosci. Nanotechnol.* **2019**, *19*, 3388−3397.

(25) Guo, Y.; Zhong, M.; Fang, Z.; Wan, P.; Yu, G. A wearable transient pressure sensor made with MXene nanosheets for sensitive broad-range human-machine interfacing. *Nano Lett.* **2019**, *19* (2), 1143−1150.

(26) Dhiman, N.; Pradhan, D.; Mohanty, P. The heteroatom (N and P) enriched nanoporous carbon as an efficient electrocatalyst for the hydrazine oxidation reaction. *Fuel* **2022**, *314*, 122722.

(27) Li, X.-r.; Jiang, Y.-h.; Wang, P.-z.; Mo, Y.; Lai, W.-d.; Li, Z.-j.; Yu, R.-j.; Du, Y.-t.; Zhang, X.-r.; Chen, Y. Effect of the oxygen functional groups of activated carbon on its electrochemical performance for supercapacitors. *New Carbon Materials* **2020**, *35*, 232−243.

(28) Daniel, S.; Praveena, M. G.; Mohammed, E. M. Exploration of Highly Photoluminescent First-Row Transition Metals (Manganese, Iron, Cobalt, Nickel, Copper, and Zinc) Co-Doped Nanocarbon Dots as Energy Storage Materials. *Mater. Sci. Eng. B* **2021**, *269*, 115145.

(29) Tiwari, P.; Jaiswal, J.; Chandra, R. Hierarchal Growth of $MoS_2$@CNT Heterostructure for All Solid State Symmetric Supercapacitor: Insights into the Surface Science and Storage Mechanism. *Electrochim. Acta* **2019**, *324*, 134767.

(30) Feng, S.; Wang, X.; Wang, M.; Bai, C.; Cao, S.; Kong, D. Crumpled Mxene electrodes for ultra-stretchable and high area capacitance Supercapacitors. *Nano Lett.* **2021**, *21*, 7561−7568.
(31) Chao, J.; Yang, L.; Liu, J.; Hu, R.; Zhu, M. Sandwiched $MoS_2$/Polyaniline Nanosheets Array Vertically Aligned on Reduced Graphene Oxide for High Performance Supercapacitors. *Electrochim. Acta* **2018**, *270*, 387−394.
(32) Singha, S. S.; Mondal, S.; Bhattacharya, T. S.; Das, L.; Sen, K.; Satpati, B.; Das, K.; Singha, A. Au Nanoparticles Functionalized 3D-$MoS_2$ Nanoflower: An Efficient SERS Matrix for Biomolecule Sensing. *Biosens. Bioelectron.* **2018**, *119*, 10−17.
(33) Gao, Y. P.; Huang, K. J.; Wu, X.; Hou, Z. Q.; Liu, Y. Y. $MoS_2$ nanosheets assembling three-dimensional nanospheres for enhanced-performance supercapacitor. *J. Alloys Compd.* **2018**, *741*, 174−181.
(34) Huang, K. J.; Wang, L.; Liu, Y. J.; Liu, Y. M.; Wang, H. B.; Gan, T.; Wang, L. L. Layered $MoS_2$−Graphene composites for supercapacitor applications with enhanced capacitive performance. *Int. J. Hydrogr. Energy.* **2013**, *38*, 14027−14034.
(35) Lin, T. W.; Sadhasivam, T.; Wang, A. Y.; Chen, T. Y.; Lin, J. Y.; Shao, L. D. Ternary Composite Nanosheets With $MoS_2$/$WS_2$/Graphene Heterostructures as High-Performance Cathode Materials for Supercapacitors. *ChemElectroChem.* **2018**, *5*, 1024−1031.
(36) Dhiman, N.; Ghosh, S.; Mishra, Y. K.; Tripathi, K. M. Prospects of nano-carbons as emerging catalysts for enzyme-mimetic applications. *Mater. Adv.* **2022**, *3*, 3101−3122.
(37) Kim, H. J.; Kim, D. J.; Anitha, T.; Yedluri, Ak.; Bak, J. S.; Cho, I.; Jagadeesh, M.; Reddy, A. E. A Facile One-Step Hydrothermal Approach for the Synthesis of a $CuMoO_4$/$MoS_2$ Composite as a High Performance Pseudocapacitive Material for Supercapacitor Applications. *New J. Chem.* **2019**, *43*, 15605−15613.
(38) Singha, S. S.; Rudra, S.; Mondal, S.; Pradhan, M.; Nayak, A. K.; Satpati, B.; Pal, P.; Das, K.; Singha, A. Mn incorporated $MoS_2$ nanoflower: A high performance electrode materials for symmetric supercapacitor. *Electrochim. Acta* **2020**, 338.
(39) Zardkhoshoui, A. M.; Davarani, S. S. H. Flexible asymmetric supercapacitors based on CuO@$MnO_2$-rGO and $MoS_2$-rGO with ultrahigh energy density. *J. Electroanal. Chem.* **2018**, *827*, 221−229.
(40) Hu, S.; Chen, W.; Zhou, J.; Yin, F.; Uchaker, E.; Zhang, Q.; Cao, G. Preparation of Carbon Coated $MoS_2$ Flower-Like Nanostructure with Self-Assembled Nanosheets as High-Performance Lithium-Ion Battery Anodes. *J. Mater. Chem. A* **2014**, *2*, 7862−7872.
(41) Sarmah, D.; Kumar, A. Layer-by-layer self-assembly of ternary $MoS_2$-rGO@PPyNTs nanocomposites for high performance supercapacitor electrodes. *Synth. Met.* **2018**, *243*, 75−89.
(42) Liu, L.; Xie, Z.; Du, X.; Yu, D.; Yang, B.; Li, B.; Liu, X. Large-Scale Mechanical Preparation of Graphene Containing Nickel, Nitrogen and Oxygen Dopants as Supercapacitor Electrode Material. *Chem. Eng.* **2022**, *430*, 132815.
(43) Zhang, W. J.; Huang, K. J. A Review of Recent Progress in Molybdenum Disulfide-Based Supercapacitors and Batteries. *Inorg. Chem. Front.* **2017**, *4*, 1602−1620.
(44) Sun, H.; Liu, H.; Hou, Z.; Zhou, R.; Liu, X.; Wang, J. G. Edge-Terminated $MoS_2$ Nanosheets with an Expanded Interlayer Spacing on Graphene to Boost Super Capacitive Performance. *Chem. Eng.* **2020**, *387*, 124204.


https://doi.org/10.1021/acs.nanolett.2c02595
*Nano Lett.* 2022, 22, 8161−8167